Finite Elements in Analysis and Design 91 (2014) 95–107

Contents lists available at ScienceDirect

Finite Elements in Analysis and Design

journal homepage: www.elsevier.com/locate/finel

A beam to 3D model switch in transient dynamic analysis

Mikhael Tannous [a,*], Patrice Cartraud [a], David Dureisseix [b], Mohamed Torkhani [c]

[a] GéM, Ecole Centrale de Nantes, France
[b] Université de Lyon, LaMCos, INSA de Lyon, CNRS UMR 5259, France
[c] LaMSID UMR EDF-CNRS-CEA 2832, EDF R&D, F-92141 Clamart Cedex, France

ARTICLE INFO

Article history:
Received 18 October 2013
Received in revised form
18 April 2014
Accepted 5 July 2014
Available online 13 August 2014

Keywords:
Transient dynamics
Finite elements
Switch

ABSTRACT

Transient structural dynamic analyses often exhibit different phases, which enable one to use an adaptive modeling. Thus, a 3D model is required for a better understanding of local or non-linear effects, whereas a simplified beam model is sufficient for simulating the linear phenomena occurring for a long period of time.

This paper proposes a method which enables one to switch from a beam to a 3D model during a transient dynamic analysis, and thus, allows one to reduce the computational cost while preserving a good accuracy.

The method is validated through comparisons with a 3D reference solution computed during all the simulation.

1. Introduction

Many transient structural dynamic problems require a 3D model in order to accurately account for local effects, that occur along a small period of time. However, a 3D model for the entire structure used during the whole simulation will result in an unaffordable computational cost even on the best nowadays computational machines and softwares. Since a 3D model is required for a better understanding of local or non-linear effects, whereas a simplified beam model is sufficient for simulating the linear phenomena occurring for a long period of time, an adaptive modeling technique in which a 3D and a beam model are used in different phases of the transient dynamic calculations can reduce the computational cost while preserving a good accuracy. We, therefore, present a method that can reduce dramatically the computational cost, for problems where the 3D non-linearities are restricted in space and time.

To solve problems for which non-linearities are restricted in time, one can use a time integration scheme switching technique. In fact, when non-linear phenomena occur, such as contact interactions, small time steps are needed to ensure an accurate modeling of the physical phenomenon. In such cases, an explicit integration method is very adapted to reduce the computational cost. However, for the complementary part of the problem which is linear, an implicit method presents the advantage of unconditional stability, thus making it possible to use larger time steps. An algorithm that enables one to switch automatically between explicit and implicit integration schemes thus significantly reduces the computational cost, see Lo et al. [1] for crash problems, Noels et al. [2,3] for structural dynamics and Noels et al. [4] for a blade/casing interaction simulation.

For phenomena that are restricted in space, i.e. to a small part of the computational domain, a wide range of methods has been developed. These approaches can be divided into exact (or direct) methods and iterative ones. In the first group we mention the static condensation techniques and the exact structural reanalysis methods, such as those used in Hirai et al. [5], the volume patch techniques such as Arlequin [6] and the beam to 3D connections or shell to 3D connections, that enable one to account accurately for local 3D phenomena, while the rest of the model is less computationally expensive thanks to the beam or shell elements [7].

Dealing with different subdomains with different models can be managed by domain decomposition techniques. The iterative domain decomposition methods can be overlapping or non-overlapping methods. In the first group, one finds that the multi-scale methods with patch, such as the finite element patches [8] and the harmonic patches [9], enable one to have a local zoom on the global domain.

Non-overlapping domain decomposition methods can be classed into three main categories [10]: the primal approaches [11], the dual approaches (FETI method, [12]), and the hybrid or mixed approaches such as FETI-DP which is an improved version of the FETI method that mixes dual and primal approaches [13]. FETI also has a multi-scale version such that used in Mobasher Amini et al. [14] for ship structures with structural details. For similar applications we also find the micro–macro approaches [15].

* Corresponding author.
E-mail address: mikhael.tannous@ec-nantes.fr (M. Tannous).

http://dx.doi.org/10.1016/j.finel.2014.07.003
0168-874X/

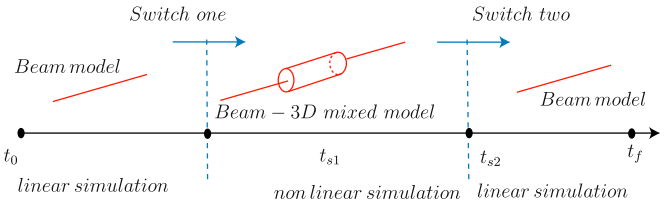

Fig. 1. Beam to 3*D* switch.

Regarding local non-linear phenomena, FETI was enhanced to deal with a large number of subdomains and can take geometric non-linearities into account Farhat et al. [16], and was adapted for contact problems in Avery et al. [17] and Dureisseix and Farhat [18]. In Gendre et al. [19,20], the authors developed an algorithm that enables one to replace the global mesh by a finely meshed local zone, in order to take local non-linear effects into consideration with low computational effort.

For problems where non-linearities are restricted both in space and in time, a strategy that allows one to use a beam model and a beam–3*D* mixed model at different stages of the transient analysis allows one to reduce the computational cost while preserving a good accuracy as illustrated in Fig. 1. In fact, the simulation starts at $t=t_0$ with a beam model for a linear simulation, and switches at $t=t_{s1}$ to a beam–3*D* mixed model before a non-linear phenomenon takes place. The simulation switches back at $t=t_{s2}$ to the beam model for the rest of the simulation that ends at t_f, if no more non-linear phenomenon is present.

This raises the problem of the switch from one model to another. This paper presents a beam to 3*D* model switch, as well as a beam to a mixed beam–3*D* model switch. The 3*D* to beam model switch is not the subject of this research work.

The main purpose of the switch method in this paper is switching from a linear transient dynamic beam problem without large rotations and with linear material behavior to a linear transient dynamic 3*D* problem. Thus, the idea is to switch from a beam to a 3*D* model before non-linear or local phenomena are to take place, in order that the 3*D* model is used for the non-linear part of the simulation. Therefore in the case where non-linearity is due to contact, the switch instant can be easily computed. In fact, when a contact is detected (the contact algorithm returns contact=1), the switch instant is computed by $t_s=t-n\times\Delta t$, where t is the contact instant, Δt is the time step value and n is a safety factor (10 is sufficient) that is taken in order to prevent the 3*D* computations from starting with an initial contact detected. However, this paper is focused on the switch process. Therefore, to demonstrate that the accuracy of the switch method is independent from the switch instant choice, this later is chosen arbitrary in the scope of our study cases.

2. Mathematical basis of the switch

A beam model simulation that started at $t=0$ is to be switched for a 3*D* model simulation at $t=t_s$. Starting with the 3*D* model at $t=t_s$ requires the collection of the beam model solution at t_s and transforming this solution to have a suitable 3*D* model initialization at the same moment.

The fundamental dynamic equation of a beam at $t=t_s$ can be written as

$$\mathbf{M}_b\ddot{\mathbf{U}}_b+\mathbf{C}_b\dot{\mathbf{U}}_b+\mathbf{K}_b\mathbf{U}_b=\mathbf{f}_b. \tag{1}$$

where $\mathbf{M}_b$, $\mathbf{C}_b$, and $\mathbf{K}_b$ are, respectively, the mass, damping and stiffness matrices of the beam model. $\mathbf{f}_b$ is the external loading at $t=t_s$, $\mathbf{U}_b$, $\dot{\mathbf{U}}_b$, and $\ddot{\mathbf{U}}_b$ denote, respectively, the beam displacements (including rotations), velocities and accelerations at the same instant.

The 3*D* model at $t=t_s$ can be described by

$$\mathbf{M}_{3D}\ddot{\mathbf{U}}_{3D}+\mathbf{C}_{3D}\dot{\mathbf{U}}_{3D}+\mathbf{K}_{3D}\mathbf{U}_{3D}=\mathbf{f}_{3D} \tag{2}$$

where $\mathbf{M}_{3D}$, $\mathbf{C}_{3D}$, and $\mathbf{K}_{3D}$ are, respectively, the mass, damping and stiffness matrices of the 3*D* model. $\mathbf{f}_{3D}$ is the external loading at $t=t_s$ on the 3*D* model, $\mathbf{U}_{3D}$, $\dot{\mathbf{U}}_{3D}$, and $\ddot{\mathbf{U}}_{3D}$ denote, respectively, the 3*D* model displacements, velocities and accelerations at the same instant.

Suppose that we start with the beam model at $t=0$ and that we want to switch to the 3*D* model at the switch moment ($t=t_s$). We have to construct the 3*D* solution $\mathbf{U}_{3D}$ from the beam solution. This is performed first by decomposing the 3*D* displacement into a cross-section rigid body displacement corresponding to the classical Timoshenko kinematical assumption $\mathbf{PU}_b$, and a 3*D* correction $\mathbf{U}_{3Dc}$ which accounts for cross-section deformation:

$$\mathbf{U}_{3D}=\mathbf{U}_{3Dc}+\mathbf{PU}_b \tag{3}$$

We therefore need to generate $\mathbf{PU}_b$ and to compute $\mathbf{U}_{3Dc}$ in order to construct the 3*D* model displacement at t_s.

2.1. Generating $\mathbf{PU}_b$

$\mathbf{PU}_b$ is obtained through a projector matrix $\mathbf{P}$ which transforms the beam displacement vector into a 3*D* rigid body displacement per beam section. It is noteworthy to say that the 3*D* mesh and the beam mesh cannot be totally disconnected in order for the switch to be done. To be able to construct the displacement of a node on the 3*D* mesh, we should have the displacements and rotations of the beam node that has the same position along the beam. In other words, the beam model should be a projection of the 3*D* mesh on its neutral axis. However, it is not easy to build $\mathbf{P}$ because it depends on the relationship between the beam mesh and the 3*D* mesh, which may change from one cross-section to another. Instead, we will generate $\mathbf{PU}_b$ as a whole.

Let N_{ij} be a node that belongs to the ith cross-section of the 3*D* model, $\mathbf{PU}_b^{ij}$ is the displacement of N_{ij} computed for a cross-section rigid body displacement. The cross-section to which belongs N_{ij} has G_i on its neutral axis. The ith beam node, which has the same coordinates as G_i, has a displacement $\mathbf{U}_b^i$ and a rotational displacement θ_b^i. We, then, compute $\mathbf{PU}_b^{ij}$ as follows:

$$\mathbf{PU}_b^{ij}=\mathbf{U}_b^i+\mathbf{N}_{ij}\mathbf{G}_i\wedge\theta_b^i \tag{4}$$

where $\mathbf{N}_{ij}\mathbf{G}_i$ is a vector oriented from N_{ij} to G_i.

2.2. Computing $\mathbf{U}_{3Dc}$

Due to the decomposition of the 3*D* displacement according to Eq. (3), the 3*D* model initialization will be performed through the 3*D* correction $\mathbf{U}_{3Dc}$. Thus, inserting Eq. (3) into Eq. (2) at ($t=t_s$) gives

$$\mathbf{M}_{3D}(\ddot{\mathbf{U}}_{3Dc}+\mathbf{P}\ddot{\mathbf{U}}_b)+\mathbf{C}_{3D}(\dot{\mathbf{U}}_{3Dc}+\mathbf{P}\dot{\mathbf{U}}_b)+\mathbf{K}_{3D}(\mathbf{U}_{3Dc}+\mathbf{PU}_b)=\mathbf{f}_{3D} \tag{5}$$

Since we have one equation with three unknowns, the following assumptions are added:

$$\dot{\mathbf{U}}_{3Dc}=\mathbf{0}$$
$$\ddot{\mathbf{U}}_{3Dc}=\mathbf{0} \tag{6}$$

They result in a displacement correction $\mathbf{U}_{3Dc}$ that corresponds to a static computation for the 3*D* model, at $t=t_s$, and that is the solution of the following equation:

$$\mathbf{K}_{3D}\mathbf{U}_{3Dc}=\mathbf{f}_{3D}-\mathbf{M}_{3D}\mathbf{P}\ddot{\mathbf{U}}_b-\mathbf{C}_{3D}\mathbf{P}\dot{\mathbf{U}}_b-\mathbf{K}_{3D}\mathbf{PU}_b \tag{7}$$

The computations of $\mathbf{P}\dot{\mathbf{U}}_b$ and $\mathbf{P}\ddot{\mathbf{U}}_b$ can be done in the same way as $\mathbf{P}\mathbf{U}_b$ by deriving Eq. (4) with respect to time, and using the beam solution for $\dot{\mathbf{U}}_b^i$, $\ddot{\mathbf{U}}_b^i$, $\dot{\theta}_b^i$ and $\ddot{\theta}_b^i$.

Now that we have in hand the 3*D* displacements at the switch instant corresponding to Eq. (3) , we can initialize the 3*D* model at $t = t_s$ by

$$\mathbf{U}_{3D} = \mathbf{U}_{3Dc} + \mathbf{P}\mathbf{U}_b$$

$$\dot{\mathbf{U}}_{3D} = \mathbf{P}\dot{\mathbf{U}}_b$$

$$\ddot{\mathbf{U}}_{3D} = \mathbf{P}\ddot{\mathbf{U}}_b \tag{8}$$

Eqs. (6) and (8) are consistent with Eq. (5), and thus allow one to initialize the 3*D* model without violating its fundamental equation of motion at the switch instant.

However, since an integration scheme is used to solve the fundamental dynamic equation, the initialization depends also on this time integration scheme, and that makes the subject of Section 3.

3. Initializing the 3*D* solution

In order to solve a dynamic problem, one needs to have in hand the initial displacements and velocities. The initial accelerations are therefore the solution of the fundamental equation of motion solved at the initial instant, in our case the switch instant. However, when this equation is solved numerically via a time integration scheme, the required initial conditions in that case depend on the time integration scheme being used. For an explicit integration scheme, not initializing the initial accelerations will lead the finite element software used (it is the case of most softwares) to consider zero initial accelerations. For an implicit integration scheme, we can correctly compute the initial accelerations that satisfy the fundamental equation of motion at that instant. Therefore, for an explicit integration scheme initializing the accelerations is mandatory to avoid an artifact transient phenomenon that may lead the integration scheme to diverge shortly after switching. However, in the examples shown in this paper, we are using an implicit integration scheme, namely a Newmark integration scheme that does not require initial accelerations since the software, Code_Aster or Abaqus, computes automatically the initial accelerations having in hand the initial displacements and velocities, as indicated in Rixen [21]. Thus in that case, the initialization of the 3*D* solution at $t = t_s$ is

$$\mathbf{U}_{3D} = \mathbf{U}_{3Dc} + \mathbf{P}\mathbf{U}_b$$

$$\dot{\mathbf{U}}_{3D} = \mathbf{P}\dot{\mathbf{U}}_b \tag{9}$$

and $\ddot{\mathbf{U}}_{3D}$ solution of

$$\mathbf{M}_{3D}\ddot{\mathbf{U}}_{3D} = (\mathbf{f}_{3D} - \mathbf{C}_{3D}\dot{\mathbf{U}}_{3D} - \mathbf{K}_{3D}\mathbf{U}_{3D}) \tag{10}$$

However, it is noteworthy to mention that with this choice only the displacements are different from the cross-section rigid-body assumption at the switch instant. The initial velocities remain those constructed from the beam model, and they are around 5% different from the 3*D* reference velocities and accelerations for most cases of study shown later in this paper. This difference seems quite small, but is still strong enough for the problems we have solved and may cause an artifact transient phenomenon depicted by high frequency oscillations in the accelerations and velocities values. These high frequency oscillations may lead the solution to diverge. In order to vanish these oscillations, one can insert a numerical damping or change the velocities corrections as detailed in below.

3.1. Numerical damping (HHT integration technique)

A numerical damping in the integration scheme can filter these high frequency oscillations without any other influence on the solution. The HHT integration scheme has been used in this study to filter the numerical oscillations. This numerical damping needs to be maintained on several time steps following the switch in order for the high frequency oscillations to vanish, as shown in the results in the following. However, we propose a more attractive method which can reduce the high frequency oscillations that appear after switching considerably and is detailed in Section 3.2.

3.2. A triple static switch procedure

As Eq. (9) shows, the high frequency oscillations are generated by a poor initialization of the velocities and subsequently of the accelerations (Eq. (10)), since the latter are generated from the beam solution and are not completely adapted to the 3*D* model. The hypothesis taken in Eq. (9) is too strong and therefore generates high frequency oscillations. However, assuming that the displacement initialization is adapted to the 3*D* model, then a strategy enabling a better initialization of the velocities (and accelerations if needed for the integration scheme) based on the displacement correction can be built with the integration scheme and thus eliminates the high frequency transient phenomenon that occurs after switching.

We, therefore, first check the displacement correction on a static problem to prove its efficiency and then, according to the integration scheme being used, construct velocity and acceleration initializations.

3.2.1. The switch for static problems

The switch for a static problem may be seen as a particular case of the dynamic one. It is investigated here to test if the 3*D* displacements after switching are close to a reference 3*D* static solution. The beam fundamental equation for a static problem is

$$\mathbf{K}\mathbf{U}_b = \mathbf{f}_b \tag{11}$$

The 3*D* fundamental equation is

$$\mathbf{K}_{3D}\mathbf{U}_{3D} = \mathbf{f}_{3D} \tag{12}$$

The 3*D* displacement can be divided as explained earlier in Eq. (3), and leads to define $\mathbf{U}_{3Dc}$ as the solution of

$$\mathbf{K}_{3D}\mathbf{U}_{3Dc} = \mathbf{f}_{3D} - \mathbf{K}_{3D}\mathbf{P}\mathbf{U}_p \tag{13}$$

This static correction $\mathbf{U}_{3Dc}$ summed with $\mathbf{P}\mathbf{U}_b$ is compared to a reference solution for the same 3*D* model mesh, computed by solving Eq. (12). This has been performed on several mesh types, cross-section shapes and boundary conditions, and the difference between the computed displacements and the reference solution has been found to be negligible, indicating that the displacements are well corrected by this switch method.

3.2.2. Basics of the triple static switch procedure

Since a static switch provides an accurate correction of the 3*D* displacements, then a correction of the velocities and accelerations can be built using three static switch procedures at three consecutive time steps. In fact, the displacement correction proposed in Section 2.2 takes the cross-section deformation into account. But the velocities proposed in Eq. (9) are for a rigid body cross-section assumption. Since we are using a Newmark integration scheme, there is no need to initialize the accelerations but we need to improve the velocities initialization. This can be achieved if the static switch is applied on three consecutive time steps, the switch instant t_s, the preceding step t_{s-1} and the following one t_{s+1}. Then based on the three successive displacements, one can

inspire from the finite difference method a better initialization of the velocities as follows:

$$\dot{\mathbf{U}}_{3D} = \frac{1}{2 \times \Delta T}([\mathbf{PU}_b + \mathbf{U}_{3Dc}]_{t_{s+1}} - [\mathbf{PU}_b + \mathbf{U}_{3Dc}]_{t_{s-1}}) \tag{14}$$

This velocity initialization combined with the displacement initialization will lead the Newmark integration scheme to compute the initial accelerations at t_s as the solution of Eq. (10).

This initialization technique proved to be simple and very efficient in the application examples shown in this paper and on several others. It is completely consistent with the Newmark integration scheme, and therefore, is proposed as a proper beam to the 3*D* model switching technique in our research work.

Note that the triple static switch procedure does not require a numerical damping. Therefore, all the following switch examples solved by a triple static switch method are not damped.

Most of our cases of study are solved with a Newmark integration scheme. However, if one wishes to use an explicit integration scheme, and as discussed earlier in this paper, initializing the accelerations is mandatory. For the central difference integration scheme, the finite difference method leads to the following initial accelerations:

$$\ddot{\mathbf{U}}_{3D} = \frac{1}{\Delta T^2}([\mathbf{PU}_b + \mathbf{U}_{3Dc}]_{t_{s+1}} - 2 \times [\mathbf{PU}_b + \mathbf{U}_{3Dc}]_{t_s} + [\mathbf{PU}_b + \mathbf{U}_{3Dc}]_{t_{s-1}}) \tag{15}$$

This acceleration initialization proved to work on several cases of study not shown in this research work.

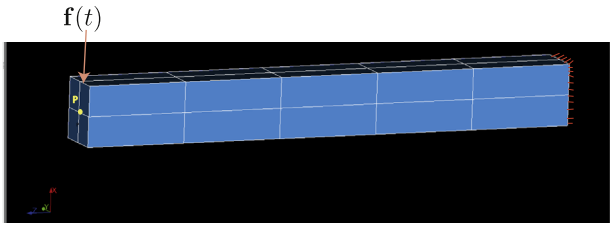

Fig. 2. The 3*D* model under study.

4. Energy consistency of the switch

To validate the concept of the switch for transient dynamic applications, we compare the 3*D* solution after switching with a 3*D* reference solution obtained by performing the same computation on the whole simulation period. Another way to check the validity of the switch method on transient dynamic problems is to check whether the switch removes or inserts parasite energy in the system at the switch instant, which can lead to non-physical simulations. Such solution precision analyses are widely used in the literature such as in Noels et al. [4,3,22], where this analysis technique served to demonstrate the stability and consistency of implicit and explicit time integration schemes switch method.

If we have a mechanical system subjected to an external force **F**, with a mass **M**, and a stiffness **K**, and if the displacements at a given instant t are denoted by **U** and the velocities at the same instant by $\dot{\mathbf{U}}$, the kinetic energy can then be written as

$$W_c = \frac{1}{2}\dot{\mathbf{U}}^T \mathbf{M}\dot{\mathbf{U}} \tag{16}$$

The strain energy reads

$$W_d = \frac{1}{2}\mathbf{U}^T \mathbf{K}\mathbf{U} \tag{17}$$

The work of the external forces W_f is computed by

$$W_f = \mathbf{F}^T \mathbf{U} \tag{18}$$

We denote W_{diss} as the work of dissipative forces (friction, damping, etc.). The kinetic energy theorem gives

$$\frac{d}{dt}W_c = \frac{d}{dt}W_f + \frac{d}{dt}(W_{diss} - W_d) \tag{19}$$

In our cases of study, the dissipative forces are negligible, then

$$W_c + W_d = W_f + cst \tag{20}$$

where *cst* is a constant that depends on the problem being solved.

We distinguish three main cases:

- **F**=**0**: the total energy $W_t = W_c + W_d$ is a constant.
- **F** is a constant: the total energy is a time dependent function (but $W_c + W_d - W_f$ is a constant).
- **F** evolves in time (which is the case of all the application examples of this paper): the total energy, is a time dependent function.

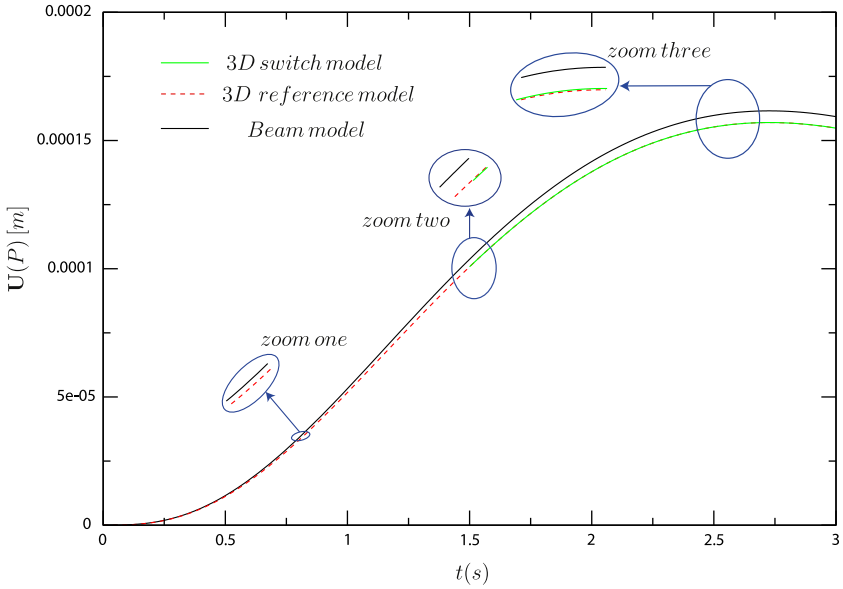

Fig. 3. Displacement results: the numerical damping method and the triple static switch lead to the same results.

To illustrate Eq. (20), let us consider a spring–mass system example. A mass M is hold by a spring having a stiffness k and subjected to an external force $\mathbf{F}$. The motion occurs along the x-axis. The displacement solution is

$$x = A\ \cos(\omega t) + B\ \sin(\omega t) + \frac{F}{k} \tag{21}$$

where $\omega = \sqrt{k/M}$. The corresponding kinetic energy is

$$W_c = \frac{1}{2}M\dot{x}^2 = \frac{1}{2}k(A^2\ \sin^2(\omega t) + B^2\ \cos^2(\omega t) - AB\ \sin(2\omega t)) \tag{22}$$

Therefore, the kinetic energy involves only the angular frequency 2ω, while the strain energy involves both ω and 2ω. In fact:

$$W_d = \frac{1}{2}kx^2 = \frac{1}{2}k(A^2\ \cos^2(\omega t) + B^2\ \sin^2(\omega t)) + \frac{F^2}{k^2} + 2AB\ \sin(\omega t)\ \cos(\omega t) + 2A\frac{F}{k}\cos(\omega t) + 2B\frac{F}{k}\sin(\omega t) \tag{23}$$

Therefore, the strain and kinetic energy do not have the same angular frequency.

If $F=0$, $W_c + W_d = \frac{1}{2}k(A^2 + B^2) = cte$.

If $F = cst \neq 0$:

$$W_c + W_d = \frac{1}{2}k(A^2 + B^2) + \frac{1}{2}\left(\frac{F^2}{k} + 2AF\ \cos(\omega t) + 2BF\ \sin(\omega t)\right) = cte + W_f \tag{24}$$

If $F=cst$, $W_t = W_c + W_d = W_f + cst$.

In this paper, the energy consistency of the switch is verified if the energy (is it the kinetic or strain energy) value of the 3D solution after switching is close to its corresponding value for the 3D reference solution. This can prove that the switch does not remove or insert energy in the 3D solution after switching. A comparison will be set between the evolution of the kinetic, strain and total energy of the beam model, the 3D reference model and the 3D switch model to prove that the switch method is energetically sound.

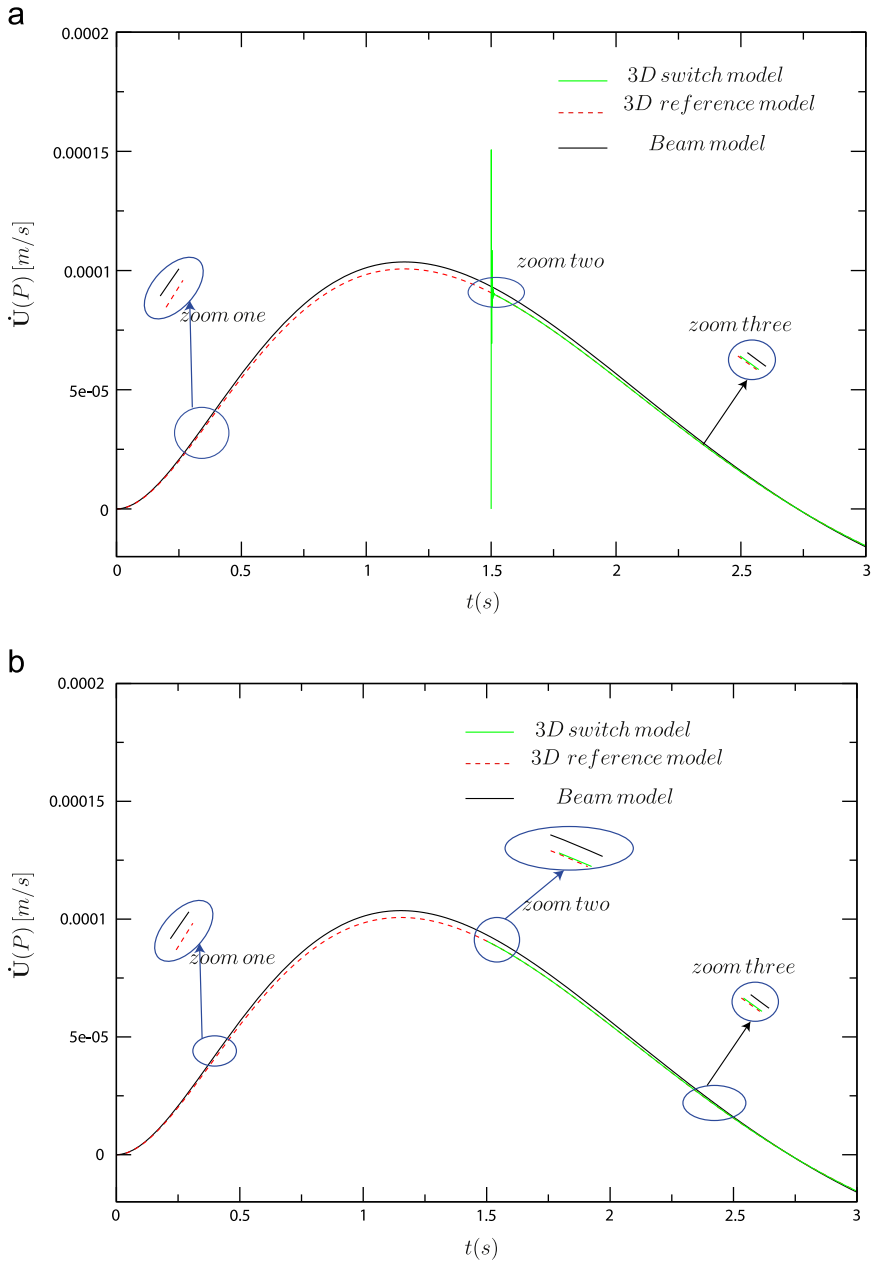

Fig. 4. Beam to 3D switch: velocity analysis. (a) Numerical damping method and (b) triple static switch procedure.

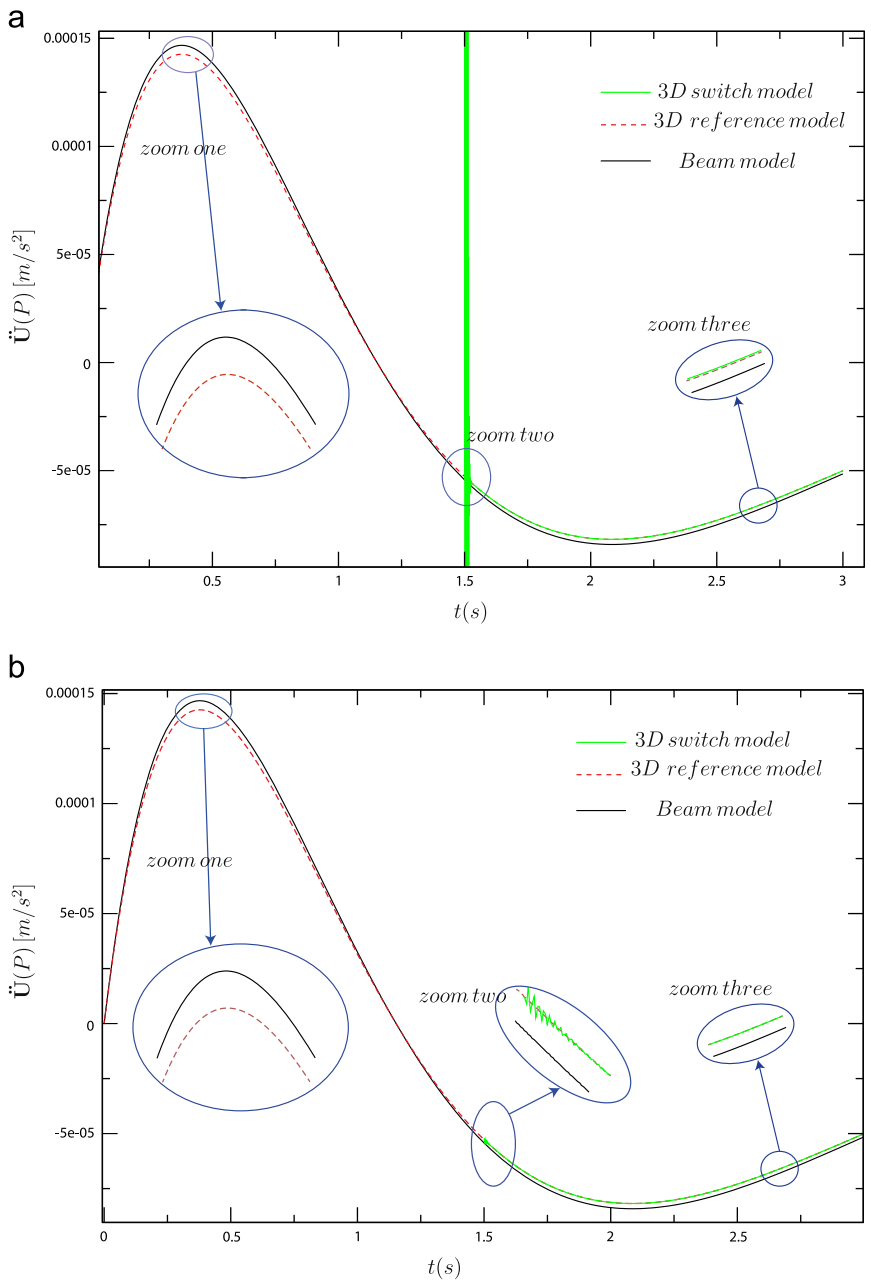

Fig. 5. Beam to 3*D* switch: acceleration analysis. (a) Numerical damping method and (b) triple static switch procedure.

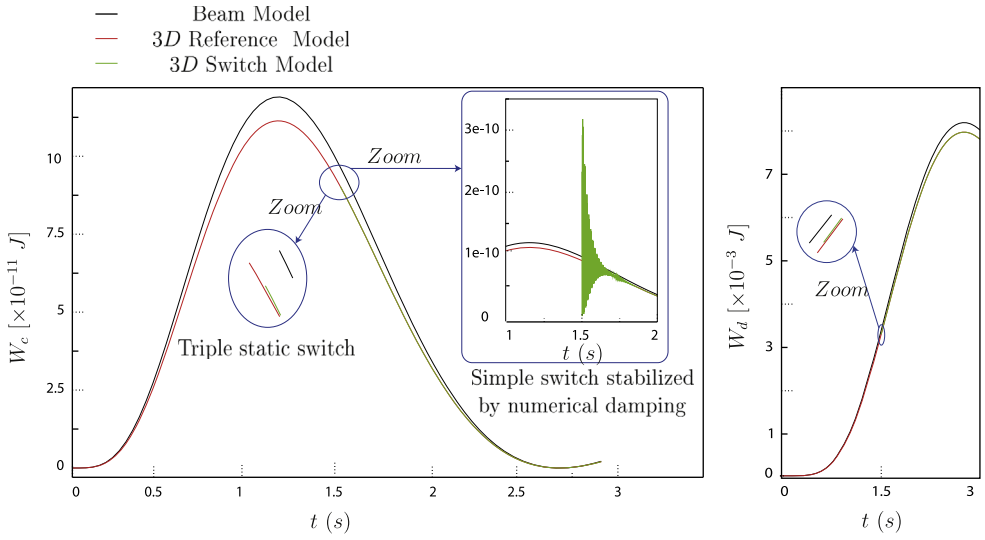

Fig. 6. The kinetic (W_c) and the strain (W_d) energy.

5. Application examples

In this section, we present a simple numerical example that illustrates the efficiency of the beam to 3*D* model switch for dynamic cases.

In fact, the method has been validated on more complex cases, for different cross-section shapes, loadings and boundary conditions. In the case considered here, the beam model is a Timoshenko beam model, with a rectangular cross-section, having the following dimensions: width 0.012 m, height 0.01 m and a length of 0.1 m. The beam is made with a steel material with density $\rho = 7800\ \mathrm{kg/m^3}$, Young's modulus $E = 2.1 \times 10^{11}\ \mathrm{N/m^2}$ and Poisson's coefficient $\nu = 0.3$. One side of the beam is fixed and the other one is subjected to a transverse load equal to $\mathbf{f}(t) = 100 \times t^3 \times e^{-1.1t}$ at its surface center. Fig. 2 illustrates the 3*D* model. The 3*D* model is quadratically meshed with approximately 1000 nodes. The switch instant is $t_s = 1.5\ s$, at which the beam simulation is switched to the 3*D* model, with the same boundary conditions and loading. The 3*D* solution after switching is compared to a reference solution, which is a 3*D* solution obtained on the same 3*D* model for a simulation that starts at $t = 0$ and last three seconds.

The switch from the beam model to the 3*D* model is performed first using the approach described in Section 2.2 (static correction with numerical damping) and second with the initialization built from the 3*D* displacements computed at three different time steps (see Section 3.2.2).

We compare the displacements, velocities and accelerations of node *P* where the load is exerted, that belongs to the 3*D* model as shown in Fig. 2, and the corresponding point that belongs to the beam model.

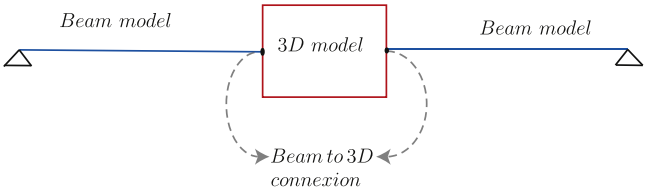

Fig. 7. Beam–3*D* mixed model.

Fig. 3 shows the displacement results. First we can see a difference between the beam solution and the 3*D* reference solution. This difference is very small, but still noticeable if we make a zoom. Immediately after switching, the 3*D* solution turns out to be very accurate and is very close to the reference one. Both switch methods exhibit practically the same precision regarding the displacements.

However, as shown in Fig. 4, which represents a velocity comparison, or Fig. 5, which represents an acceleration comparison, immediately after switching, high frequency oscillations with large amplitude occur in the case where there is only the static correction. If a numerical damping is used to filter out these oscillations, then they will be present only several time steps after switching. For a HHT integration scheme with $\alpha = 0.25$, in our case 35 time steps (0.05 s) were sufficient for the 3*D* solution to converge to the reference one. If a triple static switch procedure is performed, the velocities do not present any oscillations; however, very small oscillations occur on the accelerations and vanish very shortly after switching, see Fig. 5b

The results show that both methods work, but the triple static switch appears to be more accurate while easy to implement. The beam to 3*D* model switch accelerates the dynamic simulation of a 3*D* model while preserving a good accuracy.

Energy analysis confirms the efficiency of the switch. In fact, the switch does not remove or insert parasite energy in the solution

Fig. 6 sets a comparison between the kinetic and strain energies of the beam model, the 3*D* reference model and the 3*D* switch model. Is it the triple static switch or the simple switch stabilized by numerical damping, the same strain energy curve is obtained. However, if the simple switch is performed and is stabilized with numerical damping, oscillations are observed on the kinetic energy curve on several time steps following the switch instant before it converges to its stable value. A small difference exists between the strain energy of the 3*D* reference model and that of the beam model. That is due to modeling differences, such as the difference in the shape functions, between the beam and the 3D models. After switching, there remains a small difference between the 3*D* model strain energy and the 3*D* reference model strain energy, but it appears that the switch does not cause a disturbance on the value of the strain.

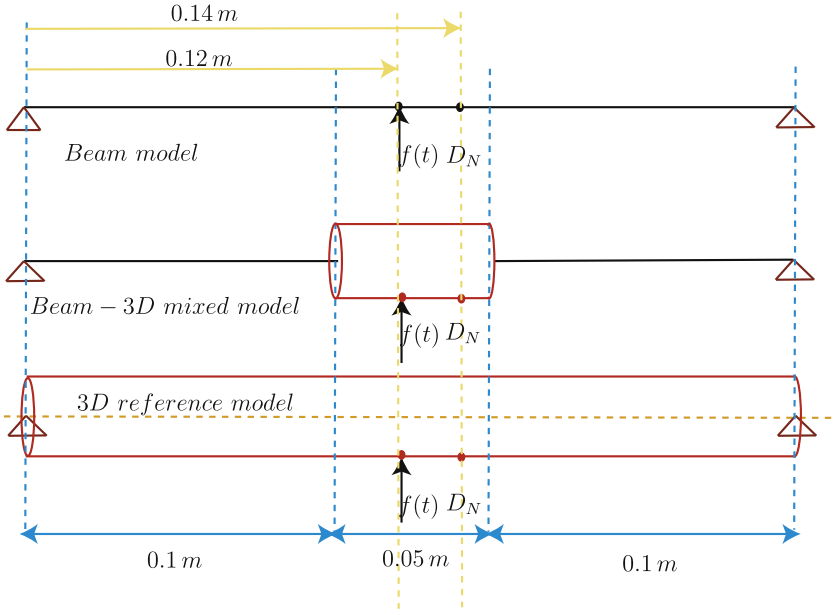

Fig. 8. Beam model, beam–3*D* mixed model, and 3*D* reference model.

This same conclusion is also obtained on the kinetic energy once the latter is stable. The triple static switch procedure is a more elegant switching technique that does not need numerical damping and does not lead to any energy perturbation even on the few time steps following the switch instant.

However, in many industrial cases, the 3*D* model is required for a small interval of time, but also for a small area. It is therefore more appropriate to switch from a beam model to a mixed beam–3*D* model. Then, the 3*D* zone is limited to the zone where local phenomena are to take place as shown in Fig. 7.

This raises the question of the beam to 3*D* connection and makes the subject of Section 6.

6. Beam to 3*D* connection

As previously mentioned in the introduction, when local phenomena are restricted in space and time, a beam to a beam–3*D* mixed model switch enables one to preserve a good modeling accuracy while decreasing the computational cost. In the following, a beam to 3*D* connection, available in Code_Aster (see [23]), is presented and will be used in this research work. This beam to 3*D* connection satisfies the consistency of the beam and 3*D* displacements (kinematic stability), as well as a suitable effort transmission from the beam to the 3*D* (static stability) that does not generate parasite strains and stresses in the connection area.

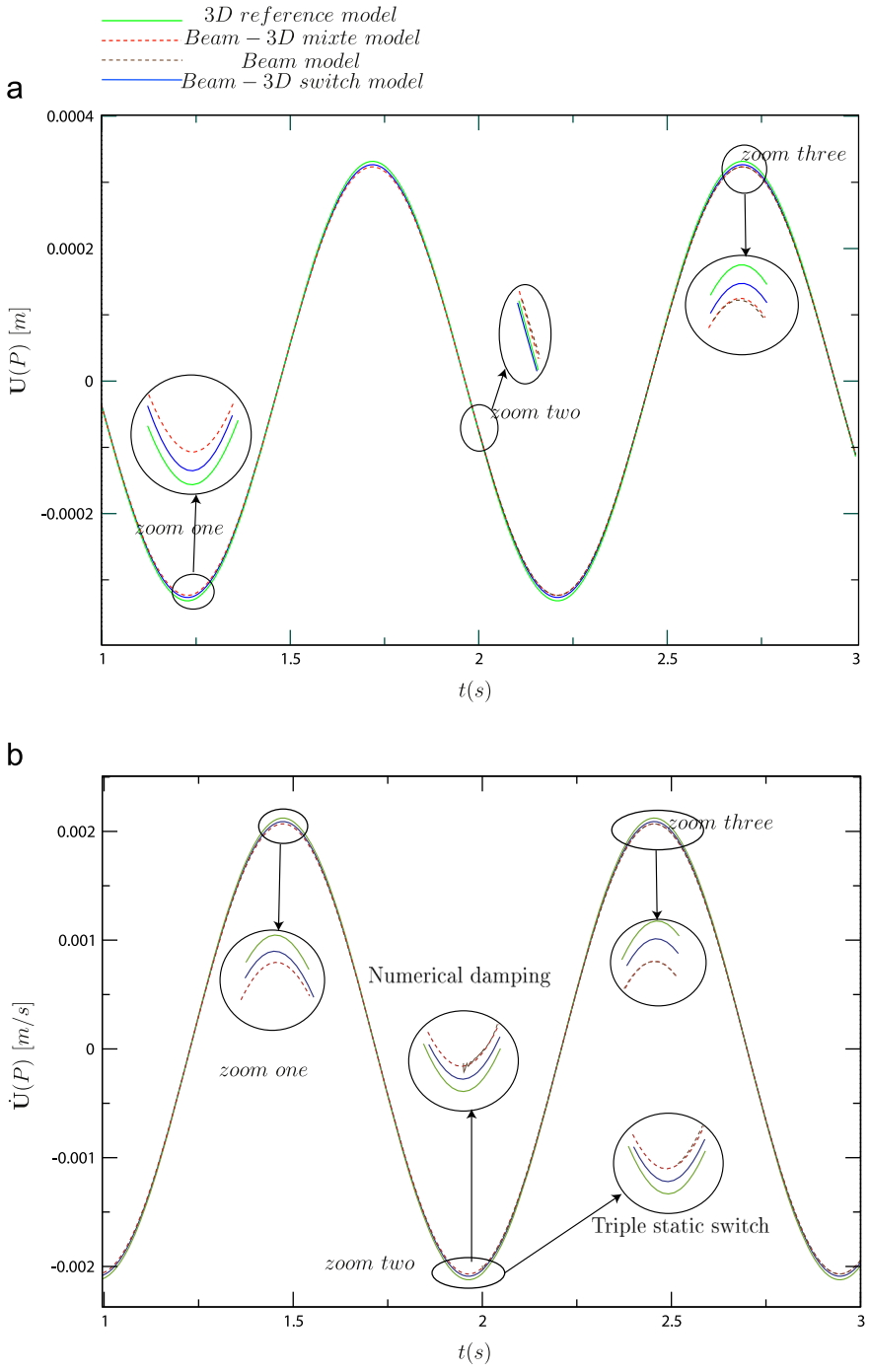

Fig. 9. Displacements and velocities analysis. (a) Displacements: the numerical damping method and the triple static switch lead to the same displacements results, (b) Velocities: comparison between the numerical damping method and the triple static switch method.

This beam to 3*D* connection is a non-overlapping one. The connection occurs between a beam node *P* and a 3*D* cross-section *S* of area *A* at the gravity center *G* of *S*.

6.1. Kinematic stability

The 3*D* displacements $\mathbf{U}_{3D}$ is the sum of a rigid-body cross-section displacement $\mathbf{U}_{3Db}$ and a cross-section deformation vector $\mathbf{U}_s$. The beam displacement and rotation vectors at point *P* are denoted, respectively, $\mathbf{U}_b$ and θ_b. The kinematic connection condition between *P* and arbitrary node *M* that belongs to section *S* reads $\mathbf{U}_{3Db} = \mathbf{U}_b + \theta_b \wedge \mathbf{GM}$.

The kinematic stability of the connection is fulfilled if the orthogonality of vectors $\mathbf{U}_{3Db}$ and $\mathbf{U}_s$ is satisfied. This ensures that the 3*D* cross-section has no influence on the displacement of the beam nodes. This can be expressed by the following equations:

$$\mathbf{U}_b = \frac{1}{A}\int_s \mathbf{U}_{3D}\, dS \tag{25}$$

$$\theta_b = I^{-1}\left(\int_s \mathbf{GM} \wedge \mathbf{U}_{3D}\, dS\right) \tag{26}$$

6.2. Static stability

In order to avoid artifact strains on the connection interface between the 3*D* model and the beam model, a suitable transmission of the loading between the beam and the 3*D* model is necessary. It can be achieved if the projection of section *S* stresses

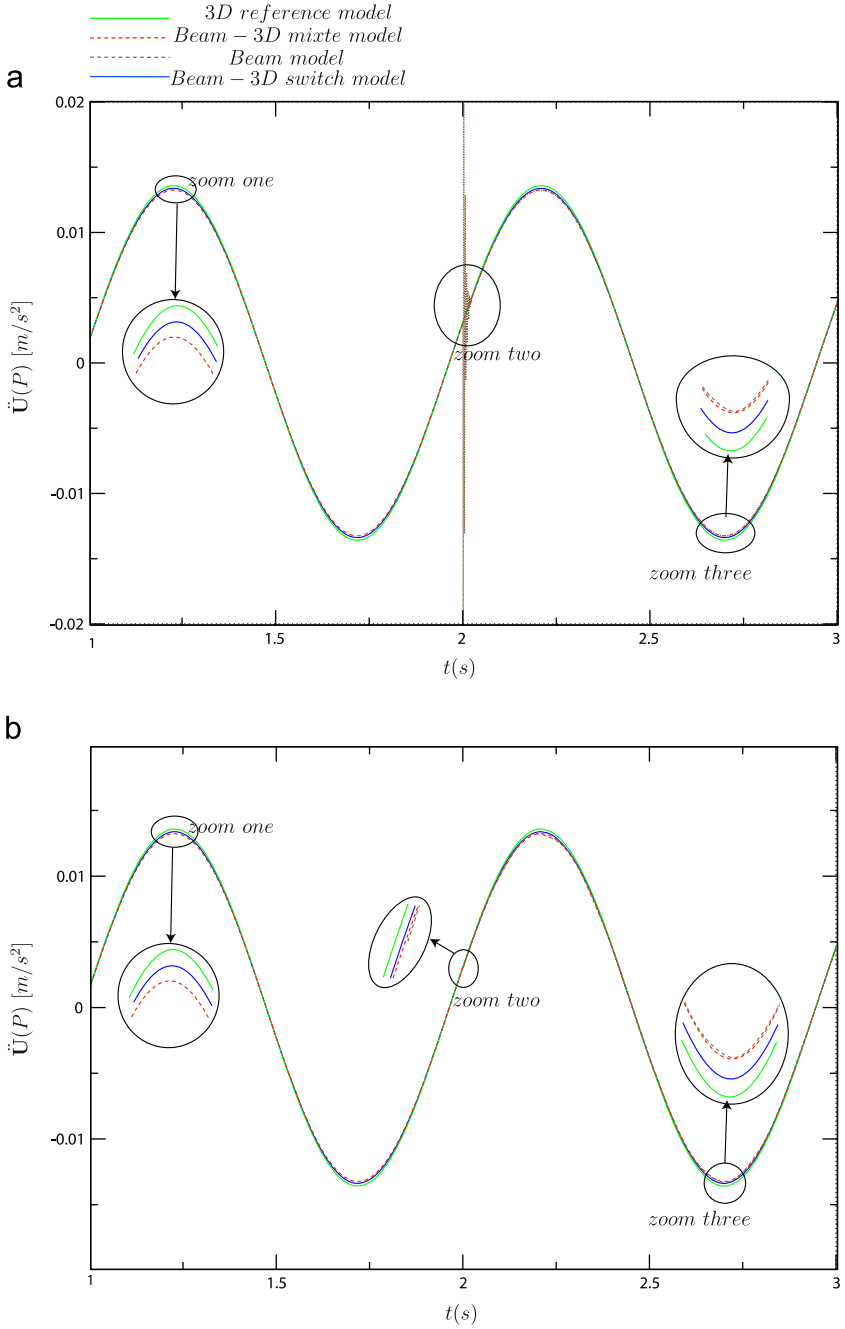

Fig. 10. Accelerations. (a) Numerical damping and (b) triple static switch.

on node P results in beam loading and is expressed by

$$\int_s \sigma \cdot n \cdot \mathbf{U}_{3D}\, dS = \mathbf{F}_p \mathbf{U}_b + \mathbf{T}_p \theta_b \tag{27}$$

where $\mathbf{F}_p$ is a loading vector on node P and $\mathbf{T}_p$ is a torque vector on node P that can be deduced from Eq. (27) by solving an optimization problem:

$$\mathbf{F}_p = \int_s \sigma \cdot n\, dS \tag{28}$$

$$\mathbf{T}_p = \int_s \mathbf{GM} \wedge \sigma \cdot n\, dS \tag{29}$$

The following section presents a beam to a mixed beam–3D model switch in transient dynamic analysis.

7. A beam to mixed beam–3D model switch example

In this example, we take a beam with a circular cross-section of radius 0.005 m and a 0.25 m length, simply supported from both sides, and that has the following material properties: $\rho = 7800$ kg/m^3, Poisson's coefficient $\nu = 0.3$ and Young's modulus $E = 2.1 \times 10^{11}$ Pa. At 0.12 m from one side it is subjected to a load of the form $\mathbf{f}(t) = -100 \times \sin(\omega \times t)$, where $\omega = 6.4$ rad/s, for a 3 s long simulation starting at $t = 0$ s. An implicit integration scheme is used with 2000 time steps. The switch instant is fixed at $t = 2$ s. For a better presentation of the results, the displacements, velocities and accelerations are presented in the following illustrations in the interval $t \in [1, 3]$ s.

The displacement, velocities and accelerations are registered with respect to time at a node D_N as illustrated in Fig. 8. The latter shows the dimensions of the model in question. The same physical model is modeled by a beam model, a whole 3D model and a

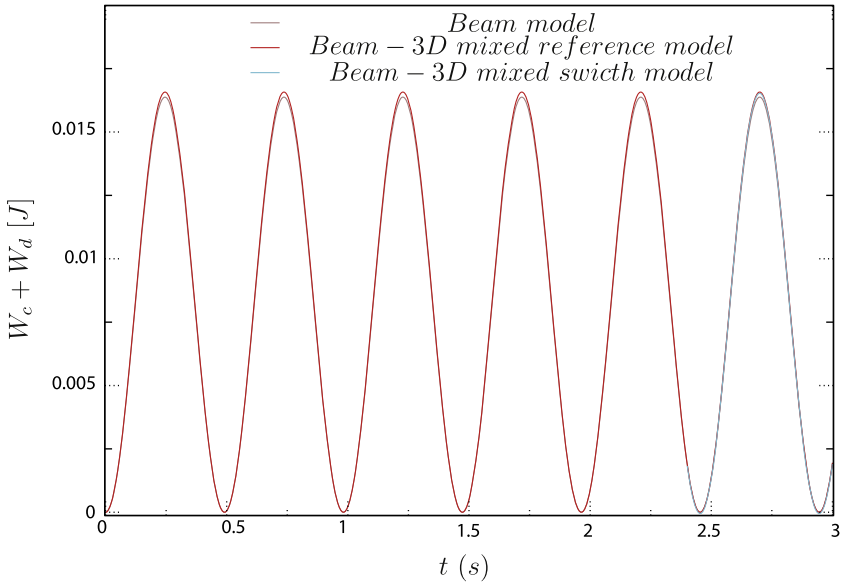

Fig. 11. Strain and kinetic energy sum.

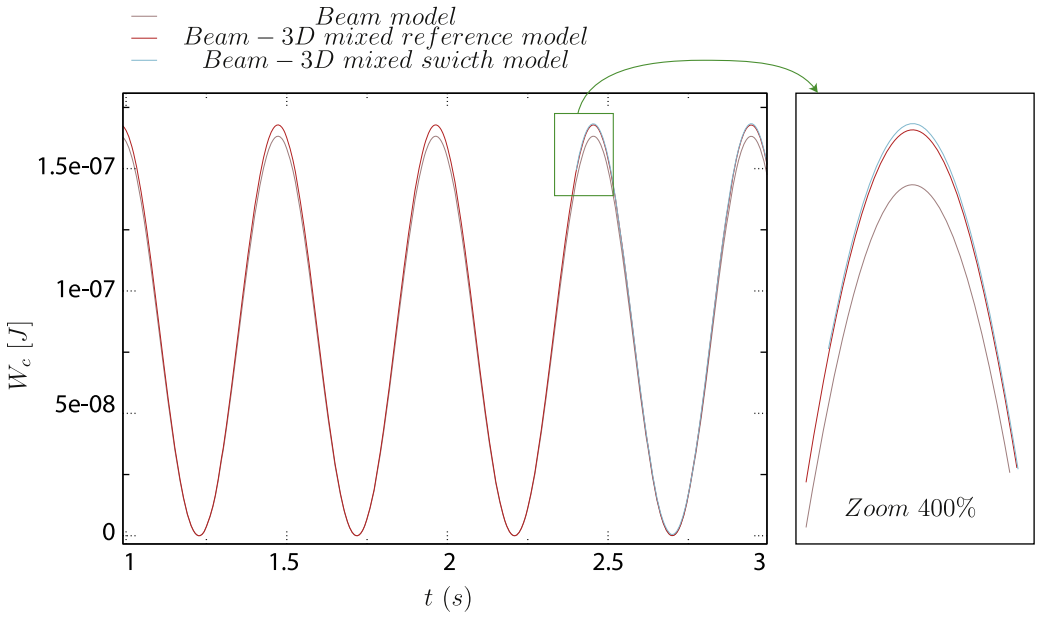

Fig. 12. Kinetic energy.

model that combines beam and 3*D* elements. The reference solution is the one computed using the 3*D* reference model. The beam to mixed beam–3*D* model switch is performed using the two initialization methods discussed earlier, namely a numerical damping method (HHT integration scheme) with $\alpha = 0.25$ and a three static switch procedure. The displacements, velocities and accelerations of the beam–3*D* mixed model after switching are compared with the beam model solution, the mixed beam–3*D* model solution and a 3*D* model reference solution, three of them for the same loading, starting at $t = 0$ s and lasting 3 s.

If a numerical damping is used to stabilize the solution after switching, a transient stage is initiated and can be seen on the accelerations, see Fig. 10a, while being less noticeable on the velocities, see Fig. 9a and absent on the displacements, see Fig. 9b.

By contrast, if a triple static switch procedure is performed, no transient stage is observed, see Figs. 9 and 10b. It is noteworthy to

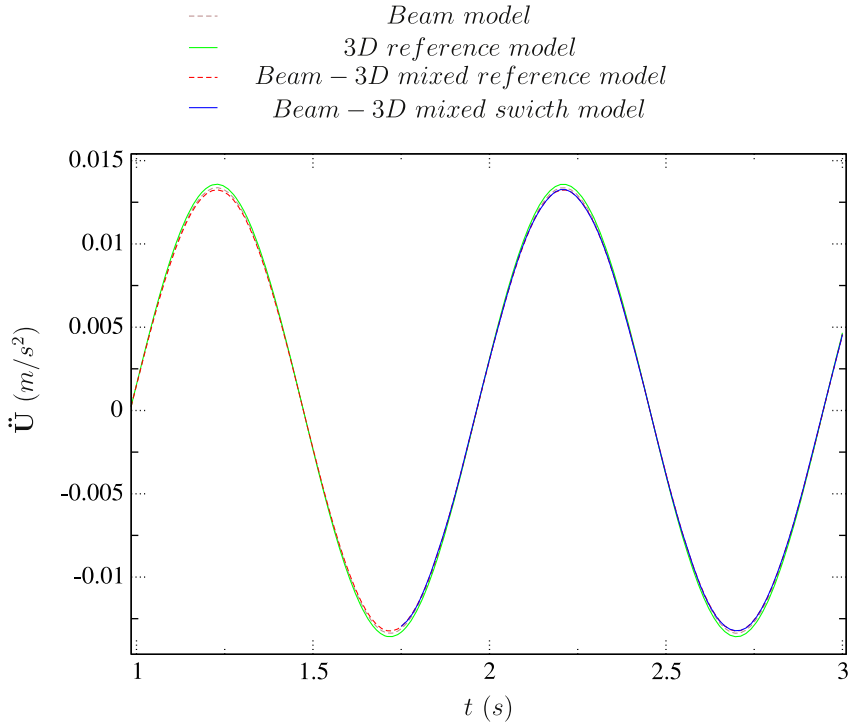

Fig. 13. Acceleration results for $t_b = 1.75$ s.

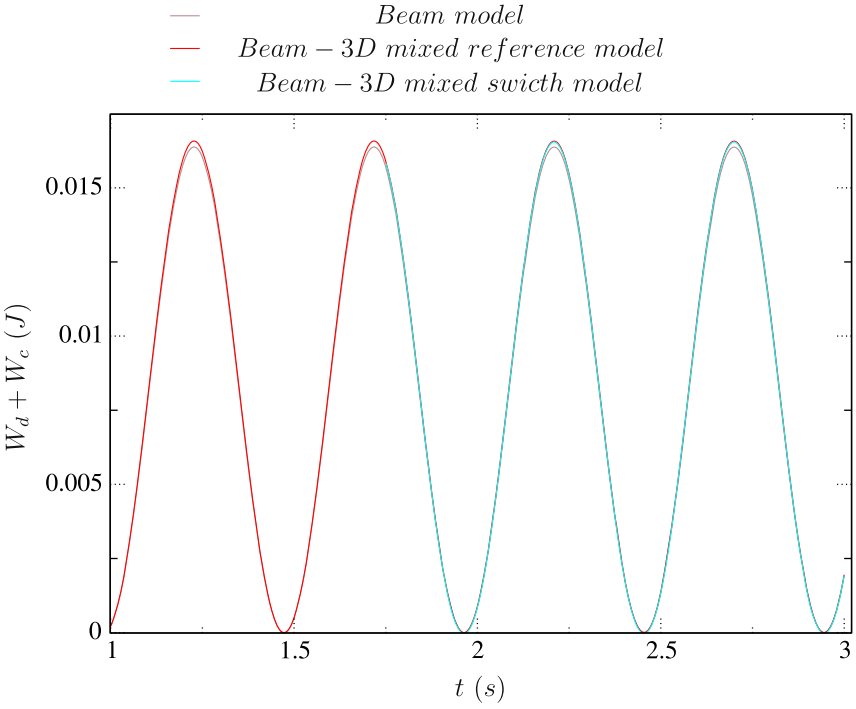

Fig. 14. Strain and kinetic energy sum at $t_b = 1.75$ s.

say that a difference exists between the displacements of the 3*D* reference model, the beam one and the beam–3*D* mixed model as shown in Fig. 9a. The beam–3*D* mixed model is closer to the beam solution, since the 3*D* zone is one-fifth the length of the beam–3*D* mixed model. This conclusion is the same for the velocities and accelerations as shown in Figs. 9b and 10.

Both switching techniques prove to be efficient. The triple static switch is more elegant while easy to implement.

We now check the energy consistency of the switch for this application example. Fig. 11 shows the sum of the kinetic and strain energy for the beam model, the mixed beam–3*D* model computed along the whole simulation time and the mixed beam–3*D* switch model. We avoid to present the energy curves corresponding to the 3*D* reference model since they do not provide essential clues for the analysis of the energy consistence of the switch.

A small difference is observed between the energy curve of the beam model and that of the mixed beam–3*D* model. This difference is due to modeling differences (shape functions differences, etc.). After switching, the mixed beam–3*D* model energy curve joins that of the reference mixed beam–3*D* model. The same conclusion drawn from the previous application example, in which no beam to 3*D* connection is used, is once more obtained: the switch does not lead to any perturbation in the energy values. The kinetic energy is presented in Fig. 12 in the time interval $t \in [1, 3]$ s, and a zoom on the kinetic energy around the switch instant is presented on the right hand side of the this same figure. Analyzing the kinetic energy curves confirms the energy consistency of the switch.

In this example, at the switch instant the velocity is near its maximum as it can be seen in Fig. 9b, while the displacements and accelerations are low as shown in Figs. 9a and 10, respectively. It is interesting to perform a switch at a different instant to have a different initial configuration such as $t_s = 1.75$ s, at which the velocities are low, while the displacements and accelerations are high. This can illustrate the efficiency of the switch and prove that the switch instant can be a random in the simulation interval. Since the triple static switch is elegant and easy to implement, we present, thereafter, the results obtained only by this method for $t_s = 1.75$ s.

Fig. 13 shows the acceleration results according to the *x*-axis at point D_N. The same accuracy is obtained on the displacements and velocities results.

Fig. 14 shows the kinetic and strain energy sum. No energy perturbation is detected. This is also the case if we check the strain and kinetic energy curves separately. It is obvious that we have the same efficiency for the switch performed at $t_s = 2.4$ s and $t_s = 1.75$ s.

8. Conclusions

We have proposed a numerical method that enables one to switch from a beam to a 3*D* model, or from a beam to a mixed beam–3*D* model, when a 3*D* description is required only on a small part of space and time domains. This technique enables one to save computational time while preserving a good accuracy.

Two switching techniques were proposed. One uses a numerical damping to filter possible artifact oscillations in accelerations and velocities, and the second, the triple static switch, is more elegant, do not need numerical damping and do not cause artifact oscillations.

The switch proved to work on dynamic and static cases. The 3*D* switch solution is practically the same as the 3*D* reference one.

The energy consistency of the switch has been demonstrated. No energy is removed or inserted by the switch.

In this paper and as also presented in Tannous et al. [24], the switch method is developed for transient dynamic analyses problems without an overall rotation. However, the main motivation behind the switch concept proposed in the Ph.D. thesis of Tannous [25], and presented in Tannous et al. [26], is its applications to turbine accidents involving rotor–stator contact interactions. The switch method will be extended, in future publications, for application to the slowing down of unbalanced turbine rotors with local interactions and frictions.

Acknowledgments

The authors thank the French National Research Agency (ANR) in the frame of its Technological Research COSINUS Program (IRINA, Project ANR 09 COSI 008 01 IRINA).

References

[1] C. Lo, T. Hinnerichs, J. Hales, Assessment of efficiency for a hybrid explicit/implicit code simulation of a multiple impact crash scenario, in: Proceedings of 2005 ASME International Mechanical Engineering Congress and Exposition, 2005, pp. 381–386.
[2] L. Noels, L. Stainier, J.-P. Ponthot, J. Boinini, Combined implicit–explicit algorithms for non-linear structural dynamics, Rev. Europ. Élém. Finis 11 (2002) 565–591.
[3] L. Noels, L. Stainier, J.-P. Ponthot, J. Bonini, Automatic time stepping algorithms for implicit numerical simulations of non-linear dynamics, Adv. Eng. Softw. 33 (2002) 589–603.
[4] L. Noels, L. Stainier, J.-P. Ponthot, J. Bonini, Automatic time stepping algorithms for implicit numerical simulations of blade/casing interactions, Int. J. Crashworthiness 6 (2001) 351–362.
[5] I. Hirai, Y. Uchiyama, Y. Mizuta, W. Pilkey, An exact zooming method, Finite Elem. Anal. Des. 1 (1985) 61–69.
[6] H. Ben Dhia, Multiscale mechanical problems: the Arlequin method, Mech. Solids Struct. 326 (1998) 899–904.
[7] P. Kettil, N.-E. Wiberg, Application of 3D solid modeling and simulation programs to a bridge structure, Eng. Comput. 18 (2002) 160–169.
[8] R. Glowinski, J. He, A. Lozinski, J. Rappaz, J. Wagner, Finite element approximation of multi-scale elliptic problems using patches of elements, J. Numer. Math. 101 (2005) 663–687.
[9] J. He, A. Lozinski, J. Rappaz, Accelerating the method of finite element patches using approximately harmonic functions, C. R. Math. Acad. Sci. Paris 345 (2007) 107–112.
[10] P. Gosselet, C. Rey, Non-overlapping domain decomposition methods in structural mechanics, Arch. Comput. Methods Eng. 11 (2005) 1–50.
[11] J. Mandel, Balancing domain decomposition, Commun. Numer. Methods Eng. 9 (1993) 233–241.
[12] C. Farhat, F.X. Roux, A method of finite element tearing and interconnecting and its parallel solution algorithm, Int. J. Numer. Methods Eng. 32 (1991) 1205–1227.
[13] C. Farhat, M. Lesoinne, P. Le Tallec, K. Pierson, D. Rixen, FETI-DP: a dual–primal unified FETI method. Part I: a faster alternative to the two-level FETI method, Int. J. Numer. Methods Eng. 50 (2001) 1523–1544.
[14] A. Mobasher Amini, D. Dureisseix, P. Cartraud, Multi-scale domain decomposition method for large-scale structural analysis with a zooming technique: application to plate assembly, Int. J. Numer. Methods Eng. 79 (2009) 417–433.
[15] P. Ladevèze, O. Loiseau, D. Dureisseix, A micro–macro and parallel computational strategy for highly heterogeneous structures, Int. J. Numer. Methods Eng. 52 (2001) 121–138.
[16] C. Farhat, K. Pierson, M. Lesoinne, The second generation FETI methods and their application to the parallel solution of large-scale linear and geometrically non-linear structural analysis problems, Comput. Methods Appl. Mech. Eng. 184 (2000) 333–374.
[17] P. Avery, G. Rebel, M. Lesoinne, C. Farhat, A numerically scalable dual–primal substructuring method for the solution of contact problems part I: the frictionless case, Comput. Methods Appl. Mech. Eng. 193 (2004) 2403–2426.
[18] D. Dureisseix, C. Farhat, A numerically scalable domain decomposition method for the solution of frictionless contact problems, Int. J. Numer. Methods Eng. 50 (2001) 2643–2666.
[19] L. Gendre, O. Allix, P. Gosselet, F. Compte, Non-intrusive and exact global/local techniques for structural problems with local plasticity, Comput. Mech. 44 (2009) 233–245.
[20] L. Gendre, O. Allix, P. Gosselet, A two-scale approximation of the Schur complement and its use for non-intrusive coupling, Int. J. Numer. Methods Eng. 87 (2011) 889–905.
[21] D.J. Rixen, Multi-body dynamics: time integration, 2002.
[22] L. Noels, L. Stainier, J.-P. Ponthot, Combined implicit/explicit time-integration algorithms for the numerical simulation of sheet metal forming, J. Comput. Appl. Math. 168 (2004) 331–339.

[23] J. Pellet, Raccord 3D—Poutre, R3.03.03., Technical Report, EDF R&D, Clamart, 2011.
[24] M. Tannous, P. Cartraud, D. Dureisseix, M. Torkhani, A beam to 3D model switch for transient dynamic analysis, in: Proceedings of the Sixth European Congress on Computational Methods in Applied Sciences and Engineering, ECCOMAS 2012, Vienna, Austria, 2012.
[25] M. Tannous, Développement et évaluation d'approches de modélisation numérique couplées 1D et 3D du contact rotor–stator (Ph.D. thesis), Ecole Centrale de Nantes, 2013.
[26] M. Tannous, P. Cartraud, D. Dureisseix, M. Torkhani, Bascule d'un modèle poutre à un modèle 3D en dynamique des machines tournantes, in: 11ème Colloque national en calcul des structures, CSMA 2013, Presqu'île de Giens, Var, 2013.